

# F1: Analysis of a Suspected Pulsar in the IR

## Finding the fundamental frequency of a pulsar

T. Harvey<sup>1</sup>

Physics and Astronomy, University of Southampton, Southampton  
e-mail: th4g18@soton.ac.uk

October 30, 2021

### ABSTRACT

**Aims.** This report aims to determine whether an observed infra-red oscillating source is characteristic of the periodic variation of a pulsar, and further to determine the fundamental frequency of oscillation.

**Methods.** The signal was analysed by using a fourier transform to produce a power spectrum for the pulsar as a function of frequency. The fundamental frequency was then further constrained by phase binning where the standard deviation was used as a measure of structure within the phase-binned signal, and the maximum was taken as a more precise estimate of the fundamental frequency. A synthetic signal was then generated using a Least Squares fit of a sinusoidal function fitted to the fundamental frequencies and higher harmonics, and the fourier transform of this was compared to the fourier transform of the original signal.

**Results.** The signal was determined to be characteristic of a pulsar given strong periodic features in the fourier transform. The fundamental frequency was estimated as  $30.3 \pm 1$  Hz from this method and the locations of the other frequency peaks were explained as either harmonics (frequency below the Nyquist limit) or shifted aliased harmonics (frequency above the Nyquist limit). The phase binning method generated an estimate of the fundamental frequency of  $29.9^{+0.42}_{-0.22}$  Hz. Both estimates were within error of each other. The generated synthetic signal had a strong qualitative resemblance to the original signal and the fourier transform recreated the aliased peaks and the relative heights of the peaks.

### 1. Introduction

Pulsars, famously discovered by Dame Jocelyn Bell Burnell in 1968 (Hewish et al. 1968), are compact pulsating EM sources. Initially discovered in the radio band, these radio pulsars had stable periodic oscillations of around 1 second. They were identified as highly magnetised, fast rotating neutron stars, with incredibly high densities up to  $10^{18} kg/m^3$  (Longair 2010). Pulsars were subsequently discovered to emit throughout the EM spectrum, including into gamma-rays.

Pulsars can rotate much faster than this, with the fastest-spinning pulsar PSR J1748-2446ad spinning at 716 Hz (Hessels et al. 2006). The theoretical limit is thought to be around 1500 Hz, where the pulsar would no longer be bound under the virial theorem and break apart (Cook et al. 1994). Pulsars with a rotational period between 1 and 10 milliseconds are known as millisecond pulsars, and are thought to be old pulsars which have been "spun-up" by the accretion of matter from a binary companion (Tauris and van den Heuvel 2006).

The extreme rotation develops as a consequence of conservation of angular momentum. A pulsar is a stellar remnant of a massive star, which collapses to around 10km in radius, a factor of  $10^{-5}$  or less of its original radius (Rybicki and Lightman 2008, Özel et al. 2009). The stars moment of inertia  $I \propto r^{-2}$  will decrease and therefore the rate of rotation will have to increase so angular momentum is conserved. The same is true of the magnetic field of the star, with the magnetic flux increasing as the radius decreases due to conservation of magnetic flux. With  $B \propto r^{-2}$ , for a sunlike star with a magnetic field of around  $10^{-2}$  T, the same  $10^{-5}$  decrease in radius would result in a magnetic field of  $10^8$  T (Longair (2010)).

Non-rotating neutron stars have an upper-mass limit given by Tolman-Oppenheimer-Volkoff (TOV) limit, initially computed

in Bombaci (1996) as  $1.5M_{\odot} < M_{ch} < 3M_{\odot}$ , and later further constrained to  $M_{ch} \approx 2.3M_{\odot}$  (Shibata et al. 2019). The limit depends on the balance between the gravitational force and the strong force repulsion of neutrons. Pulsars rotate so rapidly that the outward centripetal acceleration acts to increase this limit by 18 – 20% (Rezzolla et al. 2018, Cho 2018).

A neutron star is formed when a star  $< 20M_{\odot}$  undergoes a Type 2 SNe due to a breakdown of hydrostatic equilibrium, shedding its outer shells of hydrogen and helium as its core of heavier elements collapses. The electrons and protons in the relativistic degenerate electron gas in the core are subjected to such intense pressures during the collapse that they combine to neutrons via the process of neutronisation (inverse  $\beta$  decay).

$$p + e^- \rightarrow n + \nu_e \quad (1)$$

The neutrons cannot decay back into protons as the electron has no available states to move into. By this process almost all of the remaining matter is converted into neutrons. The exact structure of a neutron star is still the subject of much theoretical debate (Shapiro et al. 1983, Camenzind 2007, Lattimer and Prakash 2001) but they are thought to be made up almost entirely of neutrons.

Throughout the neutron star there would still be normal relativistic degenerate electron gas, which is why the magnetic field could still be generated within the star. There is significant observational evidence for these strong magnetic fields, such as the detection of cyclotron radiation from the pulsar Her X-1 in Daugherty and Ventura 1977. Camilo et al. 2000 estimates magnetic fields for two pulsars of around  $10^9$  T from the derived characteristic spin down age. Pulsars lose energy by magnetic braking (Johnston and Karastergiou 2017), causing their rotational speed to slowly decrease over time. Measurement of  $\dot{P}$  (rate of

change of period) allows direct determination of the magnetic field strength of the pulsar.

It is the misalignment of the rotation and magnetic axis that cause the characteristic "lighthouse" effect. The pulsar emits charged particles from the magnetic poles, which sweep across the sky, with one of the poles pointing along the line of sight of the observer for a fraction of every rotation. This produces a periodic sinusoidal pattern of radiation intensity which is very stable. Many pulsars have frequencies so stable they uniquely identify the pulsar, which has led to suggestions of the development of a pulsar-based GPS-like system for spacecraft (BUIST et al. 2011).

In this paper I will analyse a signal containing a potential pulsar and look for this characteristic periodic signal. I will also determine an estimate of the fundamental frequency of the pulsar using fourier analysis and phase-binning techniques.

## 2. Theory

There are a few main categories of techniques for the analysis of periodic signals.

1. Fourier methods
2. Phase-binning methods
3. least squares methods

I will explain the theory behind some of the relevant methods for determining the fundamental frequency of a pulsar.

Firstly I will look at the theoretical continuous Fourier transform, which says that a continuous signal  $F(t)$  can be converted into a signal in frequency space  $F(f)$  by the following equation where  $f$  is frequency,  $t$  is time and  $i$  is  $\sqrt{-1}$ .

$$F(f) = \int_{-\infty}^{\infty} F(t)e^{-2\pi ift} dt \quad (2)$$

There are several useful properties of the Fourier transform ( $\mathcal{F}$ ) which make it suitable for the analysis of periodic sinusoidal signals.

1. The Fourier transform is linear - for two functions A and B,  $\mathcal{F}(A + B) = \mathcal{F}(A) + \mathcal{F}(B)$ .
2. A timeshift of the  $F(t)$  function changes the phase of the signal only - the amplitude is unchanged.
3. The Fourier transform of a sinusoidal signal at frequency  $f$  is the sum of delta functions at  $\pm f$ .

This combination of properties mean that the Fourier transform of any signal which is a sum of sinusoidal signals will be delta functions at the peaks of the frequency of each individual sinusoid. The power spectrum of the fourier transform can also be computed by

$$P = |F(f)|^2 \quad (3)$$

This removes the phase component of the signal as well as the complex components of the Fourier transform. For a real input (as generally dealt with in astronomy) the power spectrum is real and even.

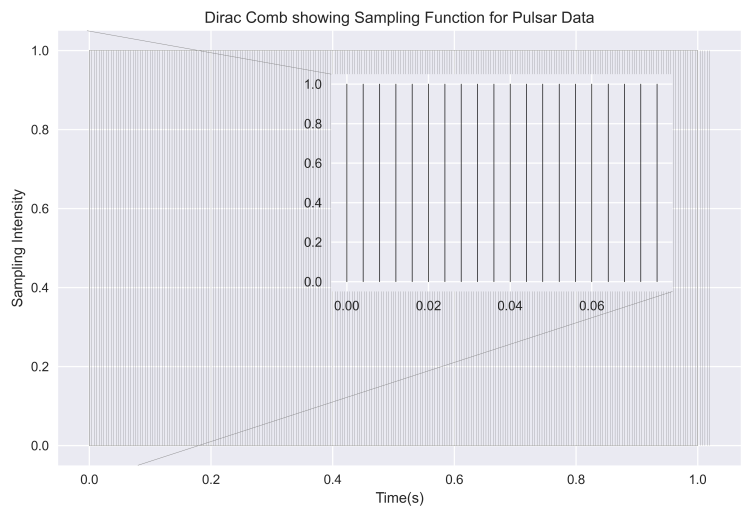


**Fig. 1.** Plot showing Dirac comb sampling function for pulsar data, with spacing every 4ms.

### 2.0.1. Convolution Theorem

Convolution (denoted by  $*$ ) is a mathematical process to produce a function from two input functions that quantifies how one function changes the shape of the other. It is equivalent to moving two functions past each other and integrating at each point. The convolution theorem states that for two functions  $a$  and  $b$

$$\mathcal{F}(a * b) = \mathcal{F}(a) \cdot \mathcal{F}(b) \quad (4)$$

and vice-versa  $\mathcal{F}(a \cdot b) = \mathcal{F}(a) * \mathcal{F}(b)$ .

Convolution is important for looking at how the way in which the data is sampled affects the resulting Fourier transform. It can be seen from the convolution theorem that the Fourier transform of the signal is the transform of the dot-product of the underlying functions in the signal. These functions include the true continuous signal, and other functions introduced by the measurement of the signal. The functions introduced by measuring the signal are known as sampling functions.

### 2.0.2. Sampling

One common form of sampling in astronomy is a window function, which quantifies the effect of sampling a continuous function for a finite time. This has the effect of replacing the Dirac delta peaks in the frequency space into sinc functions - effectively causing the very narrow delta peaks to spread out. The larger the sampling period the smaller this effect is, as the sinc functions has frequency width  $1/(N\Delta T)$  where  $N\Delta T$  is the total length of the observations (VanderPlas 2018). It also has the effect of producing small sidelobes in the data. Collectively these are known as the Window effect.

Another sampling function comes from the effect of sampling a continuous function at uniform discrete intervals, known as a Dirac comb. The sampling occurs instantaneously compared to the spacing between samples. This sampling is the product of the Dirac comb and the true signal. The Dirac comb for the observations of the pulsar can be seen in Figure 1, with spacing  $T = 4$  ms. The effect of the Fourier transform on the Dirac comb actually reproduces a Dirac comb in frequency space, with spacing  $1/T$ . This means that the fourier transform of the underlying signal is actually reproduced every  $1/T$  period in frequency space.

The only frequencies that can therefore be determined are between 0 and  $1/T$ , as every frequency outside this range is actually just a repeat (Butz 2006).

The Nyquist sampling theorem (Nyquist 1928), states that only a signal whose Fourier transforms fits between the teeth of the Dirac comb can actually be recovered by regular discrete observations of a certain period. This means that for a sinusoidal signal sampled at a rate of  $f = 1/\Delta T$ , the highest frequency that can be recovered is  $f/2$ . This is known as the Nyquist frequency (VanderPlas 2018).

The maximum range of detectable frequencies can be determined, with the upper limit being the Nyquist frequency  $f_N = 1/(2\Delta T)$ , and the lower limit  $1/(N\Delta T)$ . The effect of the sinc function also means that only differences in frequency greater than  $1/(N\Delta T)$  can be detected, which gives the frequency resolution of our Fourier transform. If the signal contains frequencies greater than that of the Nyquist frequency, they will not be correctly sampled. This is known as aliasing, and leads to repeated peaks every  $2f_N$  (Nyquist frequency), which means that some of the peaks in the data will be due to negative frequency peaks repeated every  $2f_N$ .

The effects of both of these sampling functions will be seen when analysing the Fourier transforms of discrete, finite signals.

The other consequence of analysing discrete, finite data is that the discrete fourier transform must be used which moves from an integral to a summation. The discrete Fourier transform can be written in either complex exponential form:

$$a_k = \frac{1}{N} \sum_{t=0}^{N-1} x_t e^{2\pi i kt/N} \quad (5)$$

or as a set of sinusoidal functions:

$$A_k = \frac{1}{N} \sum_{t=0}^{N-1} x_t \cos \frac{2\pi k t}{N}, \quad B_k = \frac{1}{N} \sum_{t=0}^{N-1} x_t \sin \frac{2\pi k t}{N} \quad (6)$$

where  $a_k = A_k + iB_k$  and  $k = 1 \dots N - 1$  (Altamirano 2021).

The discrete fourier transform essentially decomposes the signal into  $N$  sinusoidal waves, but half of them are mirrored in negative frequency space, meaning that actually only  $N/2$  distinct frequencies can be resolved. This is a consequence of the Nyquist sampling theorem.

Computing the Fourier transform for a large number of points is a very computationally expensive process, of order  $O(N^2)$ . Modern applications use a fast fourier transform (FFT) (Cooley and Tukey 1965) which is a  $O(N) = N \log N$  process, allowing much faster computation. The standard FFT algorithm will be used as comparison for my implementation of the Fourier transform.

### 3. Method

#### 3.1. Fourier Transform

I will be using a modified variation of the above sinusoidal fourier transform (Equation 6) which minimises the number of sinusoidal functions that need to be evaluated. It is taken from Altamirano 2021. The U coefficients are given in Equation 7, with  $U_{N+1} = U_N = 0$ ; and then computed for  $n = N - 1, N - 2 \dots 0$ .

$$U_n = x_n + 2 \cos \theta U_{n+1} - U_{n+2} \quad (7)$$

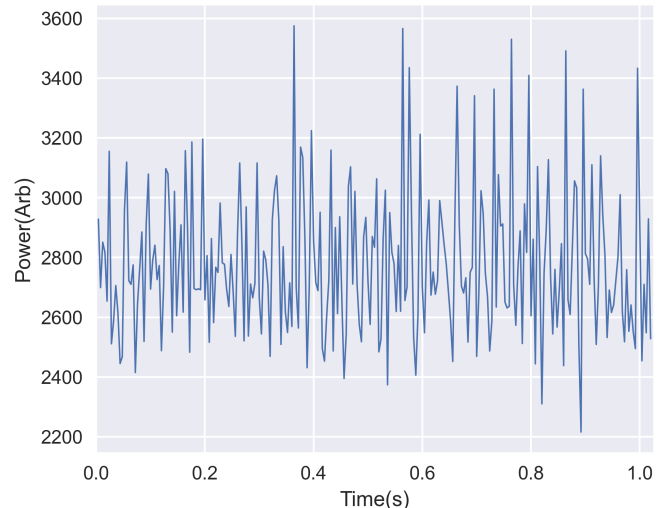


**Fig. 2.** Figure showing the pulsar intensity (in arbitrary units) as a function of time.

The two summations given above in Equation 6 can then replaced as follows:

$$\sum_{n=0}^{N-1} x_n \cos n\theta = U_0 - U_1 \cos \theta \quad \sum_{n=0}^{N-1} x_n \sin n\theta = U_1 \sin \theta \quad (8)$$

This is repeated for each value of  $k$ , with  $\theta = 2\pi k/N$ . Using Equation 3 the power at each frequency can be computed.

It is computationally faster than the traditional Fourier transform, but still much slower than the Fast Fourier transform (implemented using SciPy, Virtanen et al. 2020).

The available data consists of 256 measurements of the intensity of a region of the sky containing a potential pulsar in the infra-red, measured on an arbitrary scale every 4ms, for a total length of measurements of 1.024s. It can be seen plotted against this time scale in Figure 2.

The fourier transform algorithm is implemented using Python, along with the pandas and NumPy (Harris et al. (2020)) packages. Pandas was used to store the data in an easily accessible and iterable way, and NumPy is used for its computationally efficient arrays and trigonometric functions.

It will be used to produce a plot of power (Equation 3) vs frequency, with peaks at the fundamental frequency and subsequent harmonics. The locations of the will be estimated using a peak-finding algorithm from the SciPy signal-processing library (Virtanen et al. 2020).

#### 3.2. Phase Binning

Once I have an estimate of the fundamental frequency  $f$  of the pulsar I will use phase binning to increase the accuracy of the estimate of the fundamental frequency. The total length of the original observations is split into a number of sections, each one period of time  $\frac{1}{f}$ . The number of sections is given by the length of the signal  $T$  multiplied by the fundamental frequency. These individual sections are then further split into  $L$  bins. The number of bins used is important, as using too many bins has been shown to cause issues as for large  $L$  some of the bins do not have any points binned into them. The number of bins will be maximised to ensure the greatest waveform resolution possible

while ensuring all the bins are used. The data points in each section are binned into the L bins, with the same bins used for each section, so that all the data points are contained in one of the L bins. All the items in each bin are summed and then normalised by the number of items, then used to produce a histogram. The specifics of the maths of this can be seen in Altamirano 2021 and is not repeated here.

For the true fundamental frequency the histogram will approximate the sinusoidal shape of the true signal, and for an incorrect frequencies the binned intensities will approximately cancel out, so there will be little structure in the signal. This method should cancel out random noise in the signal, as it will not be periodic. This phase-binning technique improves the signal to noise ratio of the signal when used at the correct fundamental frequency.

The amount of structure in two signals can be compared by comparing the variation of the signal - a large variation between points and suggests there is more structure. I will use the standard deviation  $s$  because it is more resistant to outliers than a simpler method such as taking the range of the histogram. The variance is the square root of the average of the squared deviation from the mean given by

$$s = \sqrt{\frac{\sum_{\text{bins}} (X_i - \bar{X})^2}{N - 1}} \quad (9)$$

where  $X_i$  is an individual bin measurement, and  $\bar{X}$  is the mean of the bins.

For a small range around the fundamental frequency the variance of the histogram at that frequency can be computed and used to produce a plot of standard deviation vs frequency. The peak of the variance will give the fundamental frequency of the pulsar, and the full-width half maximum of the variance peak will give a measure of the uncertainty of the fundamental frequency. The full-width half maximum is the distance from the fundamental frequency when the standard deviation has decreased to half of its peak value. This will allow a more accurate estimate of the fundamental frequency and its error than Fourier Analysis provides.

### 3.3. Recreating the periodic signal

Once an estimate of the fundamental frequency is found, the periodic component of the symbol can be modelled using a series of Least-Squares fits of a periodic model of form

$$F(t, f) = C_f \sin(2\pi f(t - \phi_f)) + A \quad (10)$$

with varying amplitude  $C_f$  and  $\phi_f$ , for an oscillation around the constant value A, for the fundamental frequencies and the  $2f, 3f, \dots$  harmonics. The fit is done by the standard least squares fit - by minimising  $\chi^2$  to find the best fit at each frequency. The effect of including N harmonics is the same as computing this sum for the fit for N harmonics.

$$y = \sum_{i=1}^N C_i \sin(\omega_0 i \cdot t + \phi_i) + A \quad (11)$$

By including the higher order harmonics - including those outside the range of the Nyquist frequency, it should be possible to recreate the Fourier spectrum of the pulsar data by computing the fourier transform of the synthetic signal. This will allow me to confirm aliasing as the cause of frequency peaks in the signal. It is also a good test of the estimate of the fundamental frequency,

as if the fundamental frequency is different to the estimates the peaks will not line up. This technique is similar to that used in many of the periodogram methods, such as the Lomb-Scargle Periodogram (Astropy Collaboration et al. 2013, Astropy Collaboration et al. 2018).

## 4. Results and Discussion

### 4.1. Testing the Fourier Transform

Looking at the signal in Figure 2 there is a larger amount of variation, but by eye it is not possible to see a clear sinusoidal pattern that would be immediately suggest the signal was from a pulsar. The fourier transform will have to be used to more closely examine the signal.

Before the new fourier transform algorithm is applied to the potential pulsar data, it is useful to check that it works correctly on some test data. It produces very similar, although not precisely identical results to the FFT, as can be seen in Figure 4. Figure 4 shows the Fourier transform of a synthetic sinusoidal signal, showing the fourier power peaks at the correct frequencies for both implementations of the Fourier transform. The width and relative height of the peaks are slightly different however, although the overall signal is still very clear. The fourier transform is also still able to identify the true fundamental frequencies when the input signal is distorted by the addition of some randomly distributed noise.

### 4.2. Fourier Analysis of Pulsar Data

The theoretical limits for this data can easily be computed, given the number of data points (256) and the separation between them (4 ms). The lower limit for frequency, given in Section 2.0.2, is 0.98 Hz, and the upper (Nyquist) limit is 125Hz. The resolution in frequency space is also 0.98 Hz, so there are 128 separate frequencies that can be distinguished. Frequencies closer together than 0.98 Hz can't be distinguished given the time resolution of our data. The reason there are only 128 separate frequencies, which is  $N/2$ , is because the data is real and positive. This means it is mirrored in  $f = 0$  and so the negative half is cut-off as it doesn't have physical significance.

The fourier transform can now be applied to the data with a potential pulsar signal. The result of this can be seen in Figure 3. On the left the comparison of the SciPy FFT and my Fourier transform algorithm is shown. There are strong periodic signals in the supposed data, which suggests it is highly likely that the signal contains a pulsar. The next step is to constrain the fundamental frequency of the pulsar.

On the right the Fourier transform is shown with labelled frequency peaks. There are large peaks at  $(30.3 \pm 1)$  Hz,  $(59.6 \pm 1)$  Hz,  $(89.8 \pm 1)$  Hz,  $(99.6 \pm 1)$  Hz, and  $(121.1 \pm 1)$  Hz, along with smaller peaks at  $(41.0 \pm 1)$  Hz,  $(70.3 \pm 1)$  Hz, and  $(83.0 \pm 1)$  Hz.

Qualitatively many of the peaks are matched between the two signals, although the SciPy FFT appears to have a larger level of noise (non-zero fourier power at many frequencies.) The relative intensities of the peaks are also both similar, with both having a large peak at  $(30.3 \pm 1)$ , a maximum at  $(60.6 \pm 1)$  and similar peaks at the other harmonics.

This suggest the fundamental frequency is somewhere around  $(30.3 \pm 1)$  Hz, which explains the frequency peaks given in Table 1 for the first 4 harmonics. The table shows the expected and actual locations of the frequency peaks.

Some of the larger harmonics, which are above the 125 Hz Nyquist limit, are shown in Table 2. In Section 2.0.2, the effect of

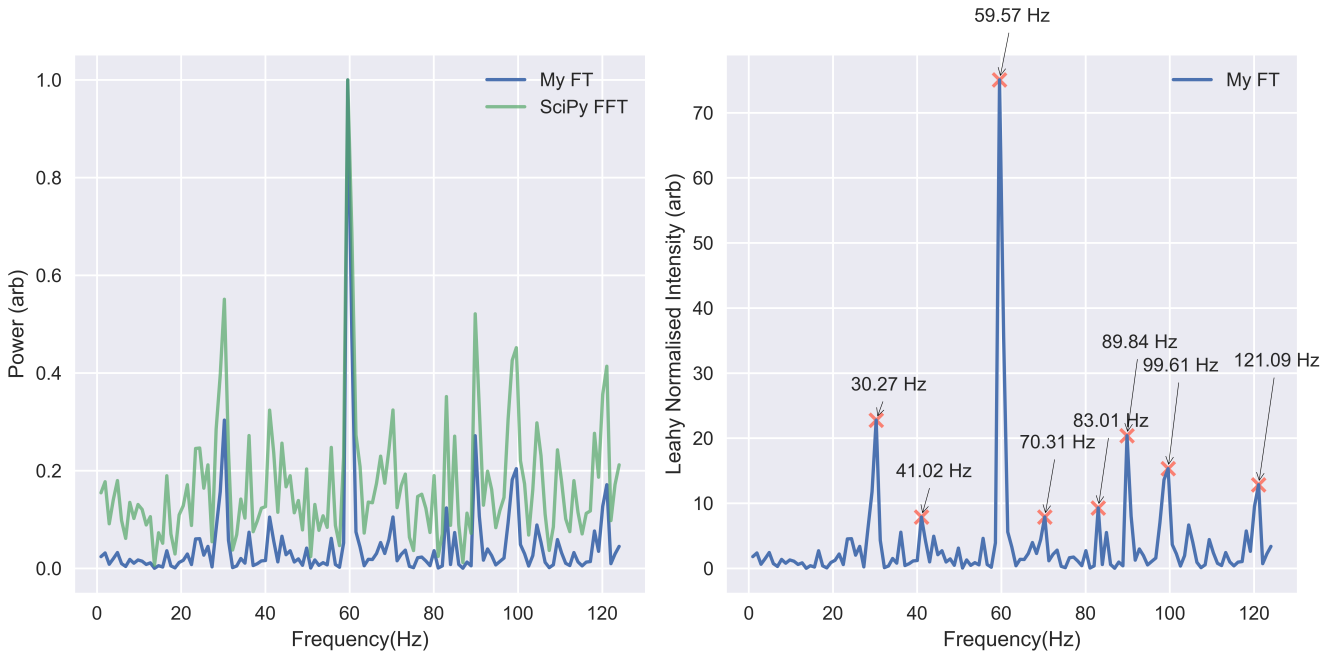


**Fig. 3.** **Figure a** (left) shows my Fourier transform and the SciPy FFT of the pulsar data as a function of frequency, with arbitrary intensity. **Figure b** (right) shows my fourier transform of the pulsar data as a function of frequency, with Leahy normalised ( $2/N$ ) intensity. The locations of intensity peaks are shown.

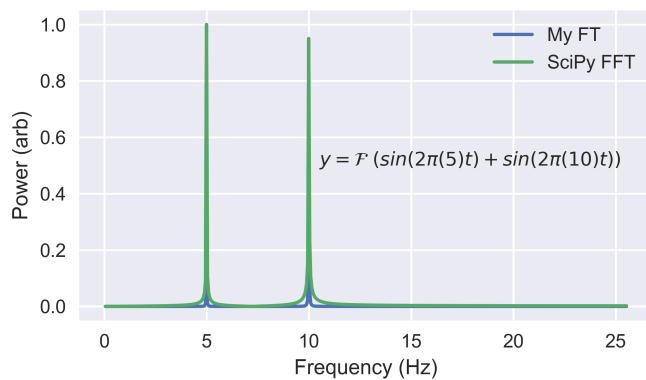


**Fig. 4.** Figure showing my Fourier Transform and the SciPy FFT for a synthetic sinusoidal signal, consisting of the sum of 2 sine waves at 5 Hz and 10Hz.

Harmonic	Expected Frequency (Hz)	Actual Frequency (Hz)
1	30.3 ( $\pm 1$ )	30.3 ( $\pm 1$ )
2	60.6 ( $\pm 2$ )	59.6 ( $\pm 1$ )
3	90.9 ( $\pm 3$ )	89.9 ( $\pm 1$ )
4	121.3 ( $\pm 4$ )	121.1 ( $\pm 1$ )

**Table 1.** Table showing actual and predicted location of first 4 harmonics given the estimate for the fundamental frequency of the pulsar.

signals above the Nyquist frequency  $f_N$  was described. It leads to an effect called aliasing, and the repetition of peaks every  $2f_N$ . Since the peaks are also reflected into negative frequency space, there will be a repeated peak at  $-f + 2f_N$  as shown in the 4<sup>th</sup> column of Table 2. The locations of these peaks are within error of observed peaks that can't otherwise be explained by harmonics (not an integer multiple of the fundamental frequency).

Harmonic	Expected Frequency (Hz)	Actual Frequency (Hz)	$-f + 2 \times f_N$ (Hz)
5	151.5 ( $\pm 5$ )	99.6 ( $\pm 1$ )	98.5 ( $\pm 6$ )
6	181.8 ( $\pm 6$ )	70.3 ( $\pm 1$ )	68.2 ( $\pm 7$ )
7	212.2 ( $\pm 7$ )	41.0 ( $\pm 1$ )	37.8 ( $\pm 8$ )
8	242.4 ( $\pm 8$ )	9.8 ( $\pm 1$ )	7.6 ( $\pm 9$ )

**Table 2.** Table showing actual and predicted location of the 5th-8th harmonics given the estimate for the fundamental frequency of the pulsar and the effect of aliasing on the shifting of the peaks. The 4th column shows the predicted location of the aliased peak (repeated every  $2f_N$ ).

#### 4.3. Phase Binning

Firstly it is useful to check that the phase-binning algorithm explained in Section 3.2 works as expected since it is a new implementation. Figure shows a noisy sinusoidal signal of known frequency. The noise is generated by adding a value taken from the normal distribution ( $\bar{x} = 0$ ,  $\sigma^2 = 1$ ) and Figure shows the result of phase binning to recreate the underlying sinusoidal wave. The phase-binned wave follows the shape of the actual wave, suggesting the phase-binning method works as expected.

Figure 7 shows the pulsar signal split into sections, defined by the estimate for the fundamental frequency  $f$  of the pulsar ( $f$  sections/second). Each section is then further split into 10 bins, shown in green.

This was then repeated for 0.1Hz frequency intervals around 30Hz, from 28 Hz to 32 Hz. It can be seen in Figure 8. There was a rough baseline of noise around a standard deviation of 40 but a clear peak at  $29.9^{+0.42}_{-0.22}$  Hz can be seen. The error is computed from the frequency difference at the half maximum of the peak of the standard deviation and the FWHM of the peak was 0.64Hz.

The waveform for any of these period-binned frequencies can be recreated, and is shown in Figure 9 for the 29.9 Hz peak. The dependence on the number of bins is also shown, as the

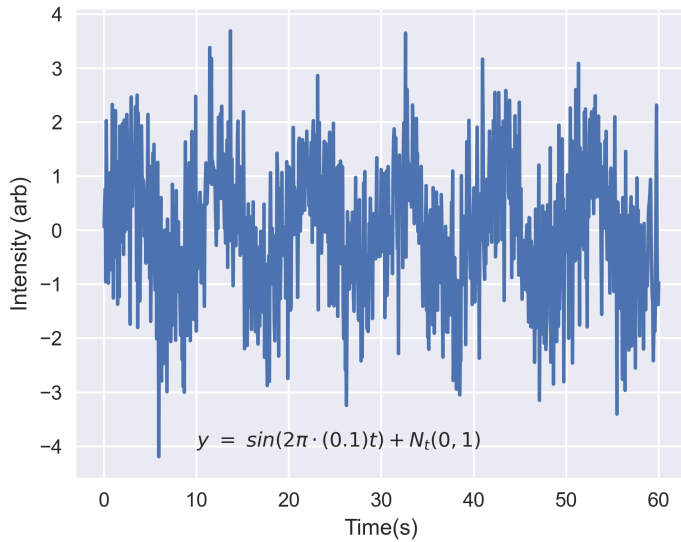


**Fig. 5.** Figure showing a synthetic sinusoidal signal (amplitude vs time) modified by the addition of some normally generated noise. Generated to show the phase-binning technique.

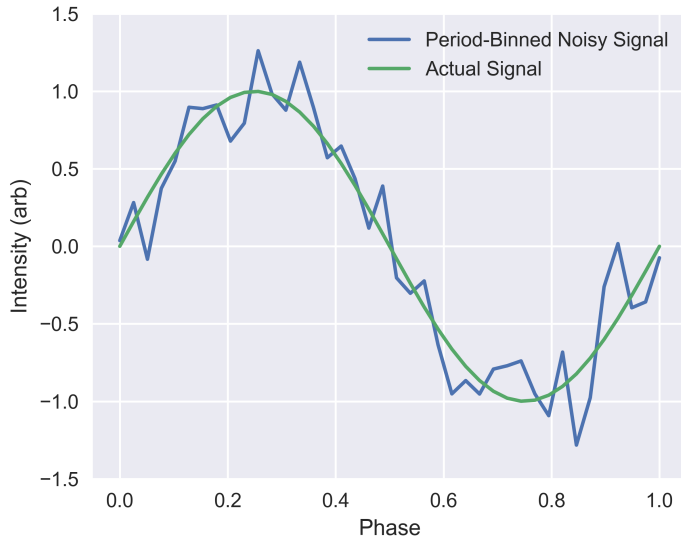


**Fig. 6.** Figure showing the signal from Figure 5 phase-binned at the known frequency of 0.1 Hz (in blue), along with the actual underlying sinusoidal signal (in green), demonstrating the efficacy of the phase-binning technique.

waveforms for integer numbers of bins between 8 and 13 are labelled.

The number of bins was chosen as 10 to recreate the highest resolution estimate of the waveform possible while also ensuring no bins were left empty. For higher frequencies greater numbers of bins left gaps in the variance graph where no points had been binned into them, leading to a 0/0 in the normalisation condition.

The number of bins can be seen to have a rather small impact on the shape of the waveform as the waveforms approximate the same sinusoidal shape for a range of bins. The exact shape of the sinusoid produced in Figure 9 is not perfectly sinusoidal for a number of reasons. Firstly the phase-binning method is not that resilient to even non-periodic noise, as can be seen in Figure 6, meaning the recreated signal will be distorted by noise in the un-

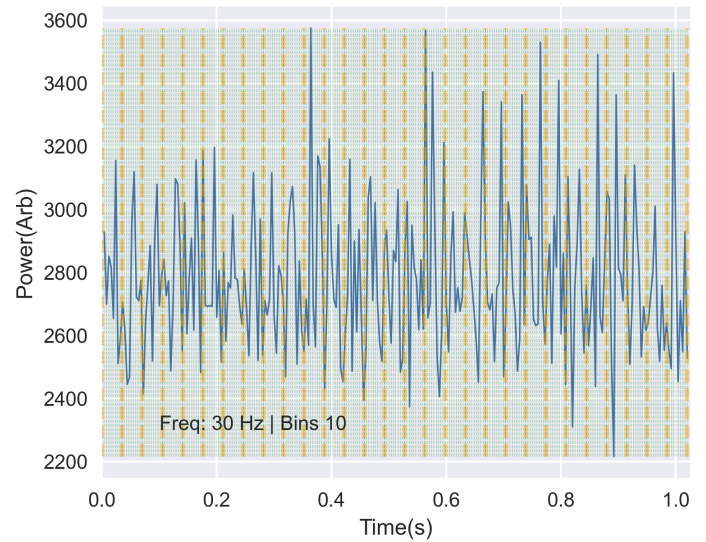


**Fig. 7.** Pulsar signal shown with the split into sections (in orange), defined by the fundamental frequency 30 Hz, and each further split into 10 bins (green).

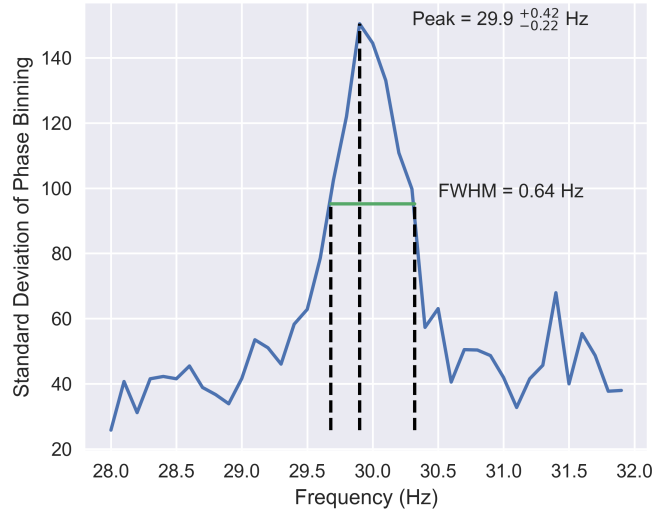


**Fig. 8.** Figure showing the peak of standard deviation around the fundamental frequency. The peak of  $29.9_{-0.22}^{+0.42}$  Hz with a FWHM of 0.64 Hz is shown. The frequency resolution is 0.1Hz.

derlying signal. Secondly the signal doesn't present as purely sinusoidal but as a superposition of harmonics, so an entirely clean sinusoidal frequency at one frequency can't be extracted due to the effect of the harmonics. Finally although the standard deviation peak is at 29.9 Hz, the errors associated mean that the true frequency could be anywhere between 29.68 Hz and 30.32 Hz and still be within error. Any frequency within this range could be used to produce a phase-binned waveform that would look qualitatively different to Figure 9. This is why the more quantitative method of measuring the standard deviation was used instead of a by-eye analysis of a set of phase-binned waveforms.

#### 4.4. Recreating the Waveform

Using the method outlined in 3.3 the pulsar signal was fitted with a sinusoidal function at the fundamental frequency and

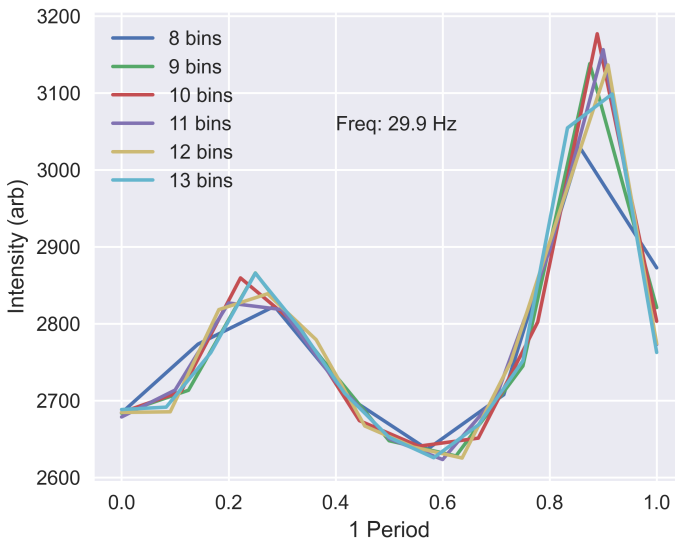


**Fig. 9.** Phase-binned wave form for 29.9 Hz, as a function of intensity vs 1 period. The effect of varying the number of bins is shown.

the higher harmonics. This fit was done using SciPy's `curve_fit` function, which uses least squares fitting to fit the free parameters (amplitude  $a_i$ , phase  $\phi_i$  and constant  $c$ , as seen in Equation 11). These fits were added together to produce a synthetic model of the actual pulsar emission as can be seen in the top graph of Figure 10. This was done up to the 12th harmonic, as above this point it was a case of diminishing returns as all the main frequency features had been recreated. The synthetic signal was generated with a very fine timestep and over a longer period of time, to approximate the continuous nature of the pulsar emission, and then the window function and sampling functions shown in the 2nd and 3rd graphs were applied to produce a signal more directly comparable to what was actually recorded as is described in the Section 2.0.2. The 4th graph shows the Fourier transform of this sampled and windowed signal. The fundamental frequency used to generate the sinusoidal signal was the  $29.9^{+0.42}_{-0.22}$  Hz estimate from the phase-binning technique since the uncertainty was smaller, and the fit was visibly better. When using multiples of 30.3 Hz the locations of some of the higher order peaks no longer precisely matched and the amplitude of the synthetic signal was smaller than the true signal.

In Figure 11 the synthetic signal and the actual signal are compared. It can be seen that many of the frequency peaks and troughs line up. The original pulsar frequency has a non-periodic variation in the magnitudes peak and trough values which is likely due to noise, which is not reproduced in the synthetic signal, however the locations of the peaks and troughs match up reasonably well. Since the locations of the higher harmonics have an increasingly larger uncertainty (as they are a multiple of the  $30.3 \pm 1$  Hz fundamental frequency) there is an error in this synthetic signal which can't easily be quantified. The finite widths of the peaks, due to the window function (see section 2.0.2), is also reproduced well since the synthetic signal is of the same length and time resolution as the original signal.

The Fourier transform of this synthetic signal can then be compared to the Fourier transform of the actual pulsar data as is shown in Figure 12. Nearly all of the significant peaks identified in Section 4.2 are recreated, which backs up the estimate of the fundamental frequency of  $29.9^{+0.42}_{-0.22}$  Hz. The relative powers of the peaks are also reproduced relatively accurately (in a

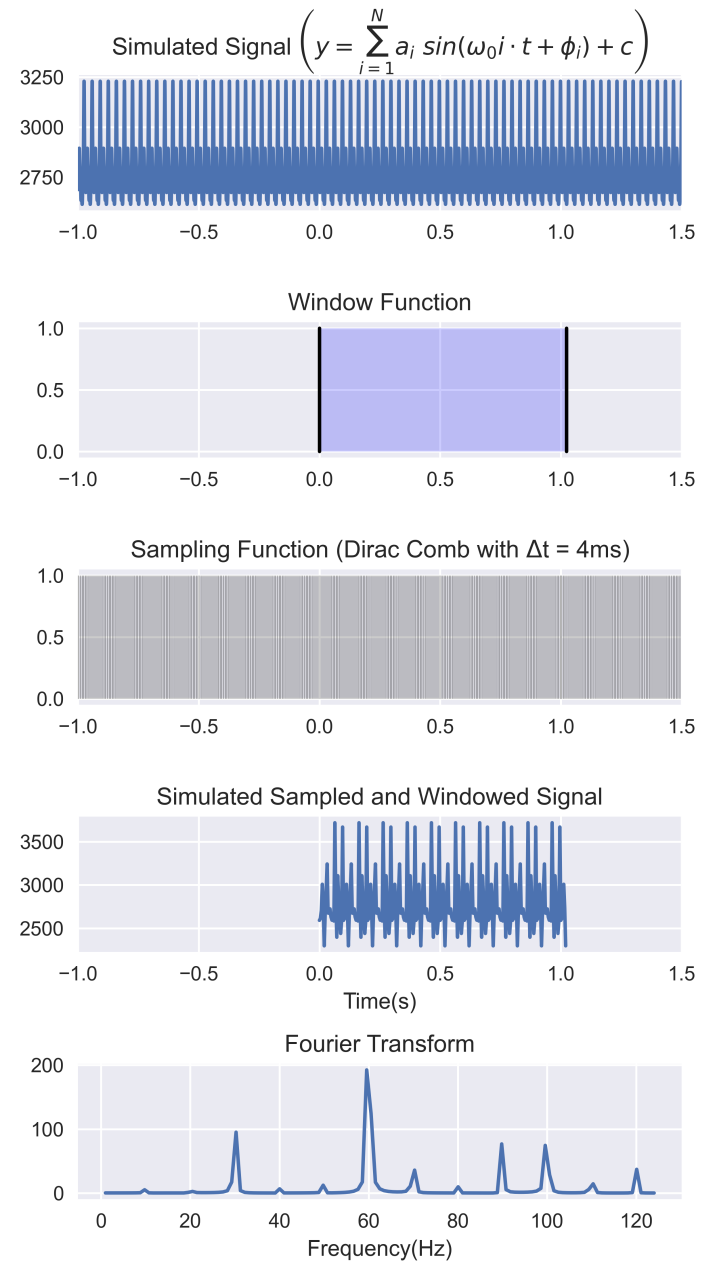


**Fig. 10.** Graphs showing the creation of a model of the periodic component of the pulsar signal. The first graph shows the continuous function along with the equation used to generate it, the 2nd and 3rd graphs show the window and sampling functions (the sampling function is a uniform comb, however the lines are too close to be displayed properly.) used to compare it to the observed pulsar signal. All x-axis until now are time in seconds. The last graph shows the Fourier transform of the synthetic signal.

qualitative sense), including the maximum at around  $(60 \pm 1)$  Hz. Several smaller peaks are not reproduced well, such as around 40 Hz and 80 Hz, and it is likely these peaks would be explained by the superposition of higher order harmonics that haven't been included. There is also a degree of noise in the original Fourier transform that isn't reproduced in the synthetic signal.

Figure 13 shows the effect of including higher harmonics on the frequency spectrum of the synthetic signal. It is the equivalent of increasing  $N$  in the sum in Equation 11. The peaks caused by each harmonic can be seen. The frequency peaks added by

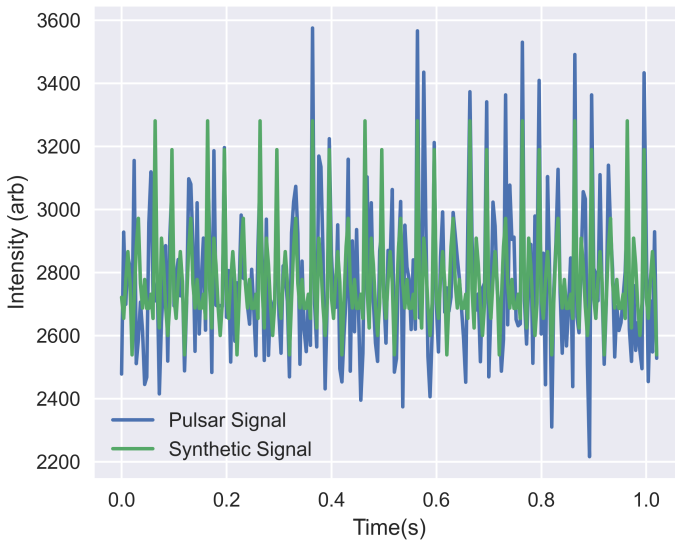


**Fig. 11.** Figure showing a comparison of the synthetic signal (green) and the actual pulsar signal (blue).

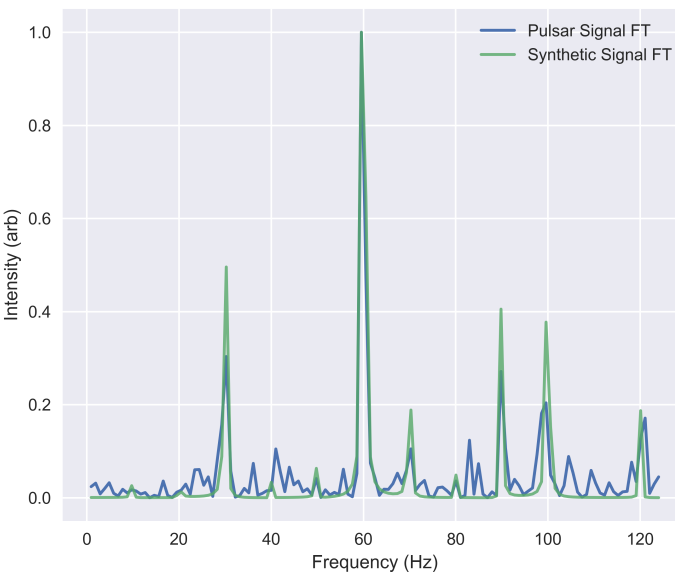


**Fig. 12.** Figure showing a comparison of the fourier transform of the synthetic signal (green) and the fourier transform of the actual pulsar signal (blue).

the inclusion of each harmonic agree with the predictions given in Table 2, suggesting the hypothesis of aliasing as the cause is correct. The peaks beyond the Nyquist limit are shifted to the frequency predicted in the table. By the 12th harmonic the fourier transform of the synthetic signal explains most of the features in the fourier transform of the pulsar signal seen in Figure 3.

From the different techniques used to estimate the fundamental frequency several slightly different results have been obtained. Firstly from the fourier analysis method the estimate was  $30.3 \pm 1$  Hz. For the phase-binning method the estimate of the fundamental frequency was  $29.9_{-0.22}^{+0.42}$  Hz. Both of these results agree as they are within error of the other, and as they are independent methods they suggest this result is credible. The generation of the synthetic signal favours the phase-binning result, as using multiples of the fourier result for the harmonics resulted in

a fourier transform with visibly shifted peaks. However due to the error on the fundamental frequencies the locations of the upper harmonics peaks have increasingly large errors so this is not a definitive result. With a fundamental frequency of this magnitude the pulsar does not spin fast enough to qualify as a millisecond pulsar, which generally have to spin between 100 and 1000 Hz (Taylor 1991).

#### 4.5. Improvements

There are a number of improvements that could be made to further constrain the fundamental frequency of the pulsar, and to learn more about it.

Firstly, if the data provided had a greater number of points (i.e. was recorded for a long period of time), at the same time resolution, the uncertainty in the fundamental frequency could be reduced. For example, if 4x as much data was available, the fundamental frequency could be constrained to less than 0.25Hz instead of 1 Hz.

If the time resolution of the data could be increased, the range of frequencies and the frequency resolution would both increase. It would be possible to probe the higher harmonics directly instead of looking at the aliased peaks.

If observations of this target were recorded accurately over a long period of time then pulsar timing techniques could be used. If the time of arrival of a pulse is measured precisely an average pulse profile can be produced by "pulse folding". This technique relies on a Lorentz transform to an inertial frame (as the Earth is orbiting the Sun). There are also corrections for pulsar dispersion and other signal delays. These measurements are used to generate a timing models to predict future pulses, and the deviations between the model and the measurements allow the investigation of unmodelled parameters, such as pulsar glitches, binary systems or orbiting exoplanets (McKee 2017). If the pulsar is timed precisely for enough time the spin down rate can be determined. To use these techniques much more info on the target would also be needed, such as its location in the sky, the instrument and telescope used to observe it, precise timing of the arrival of the signals and the associated units/uncertainties of the observations. Knowing more about the characteristics of the object, any intervening medium, and the telescope and detector used would allow for a more rigorous analysis of the uncertainties in the signal. This would also allow more research to be done on the target by cross-referencing with publicly accessible data on services like SIMBAD (Wenger et al. 2000). It would also be possible to directly cross-reference with pulsar catalogues to ensure this is a new object.

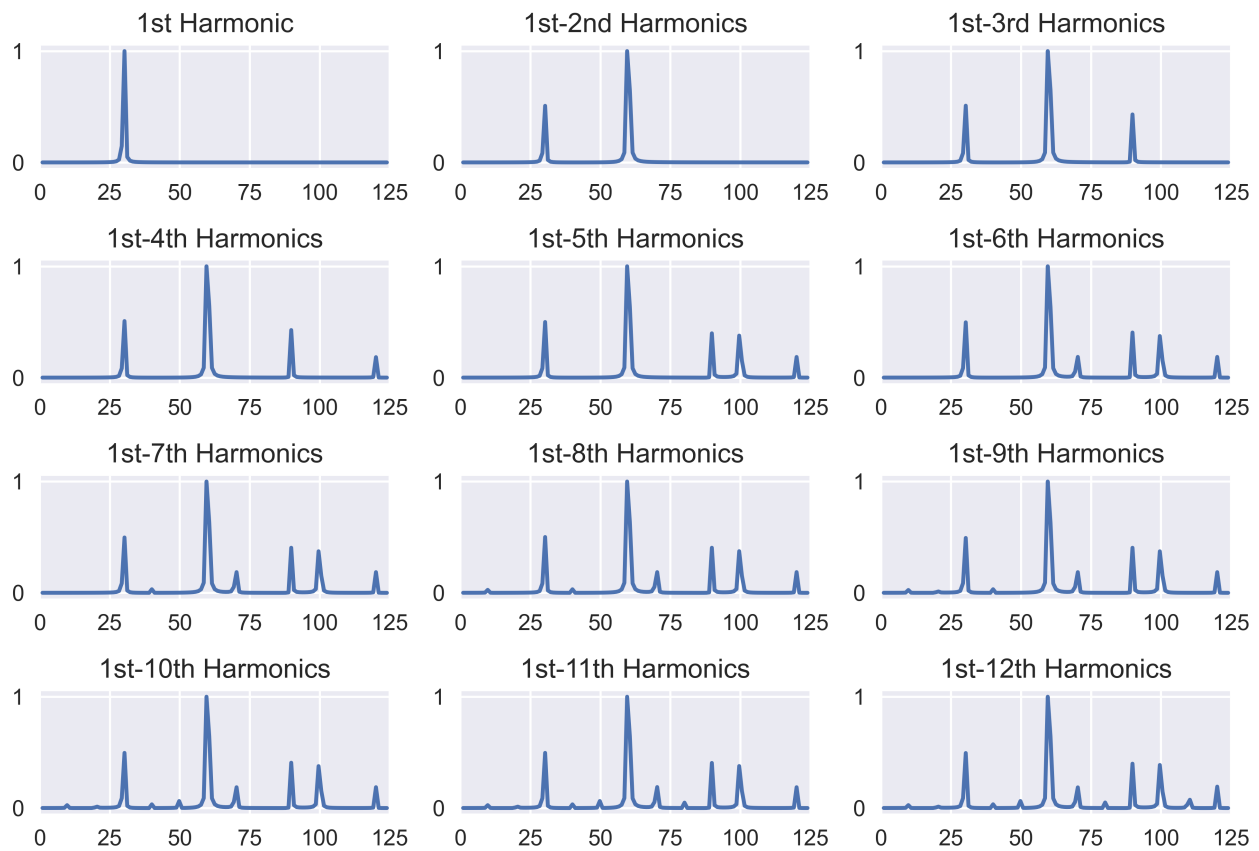


**Fig. 13.** These graphs show the fourier transform of the synthetic signal with the inclusion of increasing numbers of harmonics, demonstrating which frequency peaks are created by which harmonics. All the x-axis are Frequency in units of Hz, and the y-axis is normalised.

## 5. Conclusions

1. The fourier spectrum of a signal from a region of the sky thought to contain a pulsar has been produced.
2. The fourier spectrum has been shown to contain evidence of a sinusoidal signal oscillating at a fundamental frequency of  $30.3 \pm 1$  Hz, along with harmonics at multiples of this frequency, suggesting the presence of a pulsar.
3. The cause of frequency peaks at frequencies not an integer multiple of the fundamental frequency has been identified as the effect of aliasing from frequency peaks of harmonics above the 125Hz Nyquist frequency of the signal. The relationship between the expected frequency of the peaks and the aliased frequency is shown both in theory and experimentally.
4. Phase-binning has been used to confirm the estimate of the fundamental frequency by locating the peak of standard deviation of the signal when binned at different frequencies. The pulsar frequency was determined by this method to be  $29.9^{+0.42}_{-0.22}$  Hz which is within error of the previous estimate.
5. The periodic component of the signal has been modelled as a sum of sinusoidal waves and fitted using a Least Squares algorithm (SciPy's curve\_fit) to reproduce the underlying periodic signal.
6. The Fourier spectrum of the synthetic signal has been shown to reproduce the same locations and relative sizes of the frequency peaks as the fourier spectrum of the original pulsar data.
7. Further observations could be used to further constrain the frequency of the pulsar, and measurement of the spin down

rate could be used to estimate other properties of the pulsar, such as magnetic field strength.

## References

- Altamirano, D. (2021). *Fourier Analysis of Pulsar Data*.  
 Astropy Collaboration, Price-Whelan, A. M., Sipőcz, B. M., Günther, H. M., Lim, P. L., Crawford, S. M., Conseil, S., Shupe, D. L., Craig, M. W., Dencheva, N., Ginsburg, A., VanderPlas, J. T., Bradley, L. D., Pérez-Suárez, D., de Val-Borro, M., Aldcroft, T. L., Cruz, K. L., Robitaille, T. P., Tollerud, E. J., Ardelean, C., Babej, T., Bach, Y. P., Bachetti, M., Bakanov, A. V., Bamford, S. P., Barentsen, G., Barmby, P., Baumbach, A., Berry, K. L., Biscani, F., Boquien, M., Bostroem, K. A., Bouma, L. G., Brammer, G. B., Bray, E. M., Breytenbach, H., Buddelmeijer, H., Burke, D. J., Calderone, G., Cano Rodríguez, J. L., Cara, M., Cardoso, J. V. M., Cheedella, S., Copin, Y., Corrales, L., Crichton, D., D'Avella, D., Deil, C., Depagne, É., Dietrich, J. P., Donath, A., Droettboom, M., Earl, N., Erben, T., Fabbro, S., Ferreira, L. A., Finethy, T., Fox, R. T., Garrison, L. H., Gibbons, S. L. J., Goldstein, D. A., Gommers, R., Greco, J. P., Greenfield, P., Groener, A. M., Grollier, F., Hagen, A., Hirst, P., Homeier, D., Horton, A. J., Hosseinzadeh, G., Hu, L., Hunkeler, J. S., Ivezić, Ž., Jain, A., Jenness, T., Kanarek, G., Kendrew, S., Kern, N. S., Kerzendorf, W. E., Khvalko, A., King, J., Kirkby, D., Kulkarni, A. M., Kumar, A., Lee, A., Lenz, D., Littlefair, S. P., Ma, Z., Macleod, D. M., Mastropietro, M., McCully, C., Montagnac, S., Morris, B. M., Mueller, M., Mumford, S. J., Munoz, D., Murphy, N. A., Nelson, S., Nguyen, G. H., Ninan, J. P., Nöthe, M., Ogaz, S., Oh, S., Parejko, J. K., Parley, N., Pascual, S., Patil, R., Patil, A. A., Plunkett, A. L., Prochaska, J. X., Rastogi, T., Reddy Janga, V., Sabater, J., Sakurikar, P., Seifert, M., Sherbert, L. E., Sherwood-Taylor, H., Shih, A. Y., Sick, J., Silbiger, M. T., Singanamalla, S., Singer, L. P., Sladen, P. H., Soley, K. A., Sornarajah, S., Streicher, O., Teuben, P., Thomas, S. W., Tremblay, G. R., Turner, J. E. H., Terrón, V., van Kerkwijk, M. H., de la Vega, A., Watkins, L. L., Weaver, B. A., Whitmore, J. B., Woillez, J., Zabalza, V., and Astropy Contributors (2018). The Astropy Project: Building an Open-science Project and Status of the v2.0 Core Package. *AJ*, 156(3):123.

- Astropy Collaboration, Robitaille, T. P., Tollerud, E. J., Greenfield, P., Droetboom, M., Bray, E., Aldcroft, T., Davis, M., Ginsburg, A., Price-Whelan, A. M., Kerzendorf, W. E., Conley, A., Crighton, N., Barbary, K., Muna, D., Ferguson, H., Grollier, F., Parikh, M. M., Nair, P. H., Unther, H. M., Deil, C., Woillez, J., Conseil, S., Kramer, R., Turner, J. E. H., Singer, L., Fox, R., Weaver, B. A., Zabalza, V., Edwards, Z. I., Azalee Bostroem, K., Burke, D. J., Casey, A. R., Crawford, S. M., Dencheva, N., Ely, J., Jenness, T., Labrie, K., Lim, P. L., Pierfederici, F., Pontzen, A., Ptak, A., Refsdal, B., Servillat, M., and Streicher, O. (2013). Astropy: A community Python package for astronomy. *A&A*, 558:A33.
- Bombaci, I. (1996). The maximum mass of a neutron star. *A&A*, 305:871.
- BUIST, P. J., ENGELEN, S., NOROOZI, A., SUNDARAMOORTHY, P., VERHAGEN, S., and VERHOEVEN, C. (2011). Overview of pulsar navigation: Past, present and future trends. *NAVIGATION*, 58(2):153–164.
- Butz, T. (2006). *Fourier transformation for pedestrians*. Springer.
- Camenzind, M. (2007). *Compact objects in astrophysics*. Springer.
- Camilo, F., Kaspi, V. M., Lyne, A. G., Manchester, R. N., Bell, J. F., D'Amico, N., McKay, N. P. F., and Crawford, F. (2000). Discovery of Two High Magnetic Field Radio Pulsars. *ApJ*, 541(1):367–373.
- Cho, A. (2018). A weight limit emerges for neutron stars. *Science*, 359(6377):724–725.
- Cook, G. B., Shapiro, S. L., and Teukolsky, S. A. (1994). Recycling Pulsars to Millisecond Periods in General Relativity. *ApJ*, 423:L117.
- Cooley, J. W. and Tukey, J. W. (1965). An algorithm for the machine calculation of complex fourier series. *Mathematics of computation*, 19(90):297–301.
- Daugherty, J. and Ventura, J. (1977). Cyclotron lines in the her x-1 spectrum-structure and higher harmonics. *Astronomy and Astrophysics*, 61:723–727.
- Harris, C. R., Millman, K. J., van der Walt, S. J., Gommers, R., Virtanen, P., Cournapeau, D., Wieser, E., Taylor, J., Berg, S., Smith, N. J., Kern, R., Picus, M., Hoyer, S., van Kerkwijk, M. H., Brett, M., Haldane, A., del Río, J. F., Wiebe, M., Peterson, P., Gérard-Marchant, P., Sheppard, K., Reddy, T., Weckesser, W., Abbasi, H., Gohlke, C., and Oliphant, T. E. (2020). Array programming with NumPy. *Nature*, 585(7825):357–362.
- Hessels, J. W. T., Ransom, S. M., Stairs, I. H., Freire, P. C. C., Kaspi, V. M., and Camilo, F. (2006). A radio pulsar spinning at 716 hz. *Science*, 311(5769):1901–1904.
- Hewish, A., Bell, S. J., Pilkington, J. D. H., Scott, P. F., and Collins, R. A. (1968). Observation of a Rapidly Pulsating Radio Source. *Nature*, 217(5130):709–713.
- Johnston, S. and Karastergiou, A. (2017). Pulsar braking and the  $P-\dot{P}$  diagram. *Monthly Notices of the Royal Astronomical Society*, 467(3):3493–3499.
- Lattimer, J. M. and Prakash, M. (2001). Neutron star structure and the equation of state. *The Astrophysical Journal*, 550(1):426–442.
- Longair, M. S. (2010). *High energy astrophysics*. Cambridge university press.
- McKee, J. W. (2017). High-precision pulsar timing. *University of Manchester*.
- Nyquist, H. (1928). Certain topics in telegraph transmission theory. *Transactions of the American Institute of Electrical Engineers*, 47(2):617–644.
- Rezzolla, L., Most, E. R., and Weih, L. R. (2018). Using Gravitational-wave Observations and Quasi-universal Relations to Constrain the Maximum Mass of Neutron Stars. *ApJ*, 852(2):L25.
- Rybicki, G. B. and Lightman, A. P. (2008). *Radiative processes in astrophysics*. John Wiley & Sons.
- Shapiro, S. L., Teukolsky, S. A., Holes, B., Dwarfs, W., and Stars, N. (1983). The physics of compact objects. *New York: John Wiley & Sons*.
- Shibata, M., Zhou, E., Kiuchi, K., and Fujibayashi, S. (2019). Constraint on the maximum mass of neutron stars using gw170817 event. *Physical Review D*, 100(2).
- Tauris, T. M. and van den Heuvel, E. P. J. (2006). *Formation and evolution of compact stellar X-ray sources*, volume 39, pages 623–665.
- Taylor, J. H. (1991). Millisecond pulsars: nature's most stable clocks. *Proceedings of the IEEE*, 79(7):1054–1062.
- VanderPlas, J. T. (2018). Understanding the lomb-scargle periodogram. *The Astrophysical Journal Supplement Series*, 236(1):16.
- Virtanen, P., Gommers, R., Oliphant, T. E., Haberland, M., Reddy, T., Cournapeau, D., Burovski, E., Peterson, P., Weckesser, W., Bright, J., van der Walt, S. J., Brett, M., Wilson, J., Millman, K. J., Mayorov, N., Nelson, A. R. J., Jones, E., Kern, R., Larson, E., Carey, C. J., Polat, İ., Feng, Y., Moore, E. W., VanderPlas, J., Laxalde, D., Perktold, J., Cimrman, R., Henriksen, I., Quintero, E. A., Harris, C. R., Archibald, A. M., Ribeiro, A. H., Pedregosa, F., van Mulbregt, P., and SciPy 1.0 Contributors (2020). SciPy 1.0: Fundamental Algorithms for Scientific Computing in Python. *Nature Methods*, 17:261–272.
- Wenger, M., Ochsenbein, F., Egret, D., Dubois, P., Bonnarel, F., Borde, S., Genova, F., Jasiewicz, G., Lalòë, S., Lesteven, S., and Monier, R. (2000). The SIMBAD astronomical database. The CDS reference database for astronomical objects. *A&AS*, 143:9–22.
- Özel, F., Güver, T., and Psaltis, D. (2009). THE MASS AND RADIUS OF THE NEUTRON STAR IN EXO 1745–248. *The Astrophysical Journal*, 693(2):1775–1779.